Synthesis and Interface Structures of Zinc Sulfide Sheathed Zinc−Cadmium Nanowire Heterojunctions

ARTICLE *in* THE JOURNAL OF PHYSICAL CHEMISTRY B · AUGUST 2006

Impact Factor: 3.3 · DOI: 10.1021/jp0627832 · Source: PubMed

4 AUTHORS, INCLUDING:

Guozhen Shen
Chinese Academy of Sciences
217 PUBLICATIONS **7,225** CITATIONS
SEE PROFILE

Dmitri Golberg
National Institute for Materials Science
640 PUBLICATIONS **22,580** CITATIONS
SEE PROFILE

Synthesis and Interface Structures of Zinc Sulfide Sheathed Zinc−Cadmium Nanowire Heterojunctions

Guozhen Shen,* Yoshio Bando, Yihua Gao, and Dmitri Golberg

Nanoscale Materials Center, National Institute for Materials Science (NIMS), Namiki 1-1, Tsukuba, Ibaraki 305-0044, Japan

Received: May 7, 2006; In Final Form: June 1, 2006

Zinc sulfide (ZnS) sheathed zinc (Zn)−cadmium (Cd) nanowire heterojunctions have been prepared by thermal evaporating of ZnS and CdS powders in a vertical induction furnace at 1200 °C. Studies found that both the Zn and Cd subnanowires, within a single nanoheterojunction, are single-crystallines with the growth directions perpendicular to the $[2\bar{1}\bar{1}0]$ plane, whereas the sheathed ZnS is polycrystalline with a thickness of ca. 5 nm. The Zn/Cd interface structure in the ZnS sheathed Zn−Cd nanowire heterojunctions was thoroughly experimentally studied by high-resolution transmission electron microscopy and theoretically studied using a near-coincidence site lattice (NCSL) concept. The results show that the Cd and Zn have a crystalline orientation relationship as $[0001]_{Zn}//[0001]_{Cd}$, $(10\bar{1}0)_{Zn}//(10\bar{1}0)_{Cd}$, $(01\bar{1}0)_{Zn}//(01\bar{1}0)_{Cd}$, and $(\bar{1}100)_{Zn}//(\bar{1}100)_{Cd}$.

1. Introduction

One-dimensional (1D) nanostructures, such as nanowires, nanotubes, and nanobelts have attracted much attention as a result of their exceptional properties, which are different from bulk materials.[1−6] Among 1D nanostructures, 1D heterostructures with modulated compositions and interfaces have recently become of particular interest with respect to potential applications in nanoscale building blocks of future optoelectronic devices and systems,[7−9] and these kinds of nanostructures provide additional opportunities for enhancing the functionality of 1D nanostructures and may find applications in nanoscale heterostructured electronic devices, etc. For example, core−shell and core−multishell nanowire heterostructures can be used to fabricate high-performance coaxially gated field-effect transistors.[9] Core−shell ZnO/SnO_2 heterostructures make it possible to tailor the optical properties of nanostructures.[10] To date, diverse heterostructures assembled in either axial or radial directions have been fabricated, including semiconductor nanowire superlattices,[11−13] coaxial nanocables,[9,10−15] nanotypes,[16] metal/semiconductor nanowire heterojunctions,[17−19] metal/insulator nanocables,[20,21] and so on.[22−24]

The II-B metals, such as Zn and Cd, are important materials used in many fields. For example, Zn is a conventional type-I superconductor with a transition temperature of 0.85 K (at $H = 0$ Oe) and a critical magnetic field of 50 Oe. The superconductivity of 1D Zn nanowires shows a clear crossover from bulklike to quasi-1D behavior.[25] Cd is extensively used in nickel−cadmium and solar batteries and in pigments.[26] However, it is difficult to synthesize nanosized Cd structures using vapor phase techniques due to the relatively low melting point (mp = 312 °C[27]). Upon connection of one II-B metal to another II-B metal, unique metal−metal nanoscale contact can be formed, and it is expected that unique properties may be observed if these kinds of 1D heterostructures are fabricated.

In this work, we designed a one-step thermochemical process through evaporating ZnS and CdS powders in a graphite crucible and successfully fabricated uniform ZnS sheathed Zn−Cd nanowire heterojunctions, which contain both metal−metal subjunctions and metal−semiconductor subjunctions within a single nanowire heterojunction. We also present a thorough analysis of their morphological and structural characteristics.

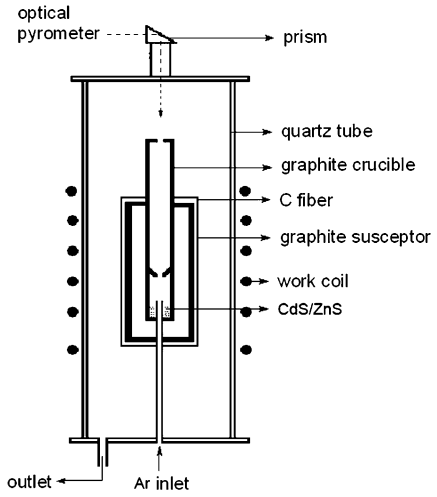

Figure 1. Schematic illustration of the furnace used in the experiment.

2. Experimental Section

The ZnS sheathed Zn−Cd nanowire heterojunctions were synthesized in a vertical induction furnace, as shown in Figure 1. The furnace consisted of a fused-quartz tube and an induction-heated cylinder made of high-purity graphite coated with a carbon-fiber thermoinsulating layer. The furnace had one inlet and one outlet on its base. A graphite crucible, containing a mixture of ZnS (1.2 g) and CdS (0.8 g) powders, was placed at the center cylinder zone. After evacuation of the quartz tube to ∼20 Pa, a pure Ar flow was introduced and maintained through the inlet at a flow rate of 200 sccm at ambient pressure in the furnace, and the crucible was rapidly heated and kept at ∼1200 °C for 1 h. After the reaction was terminated and the furnace

* To whom correspondence should be addressed. E-mail: SHEN.guozhen@nims.go.jp. Fax: 81-29-851-6280.

10.1021/jp0627832 CCC: $33.50
Published on Web 07/04/2006

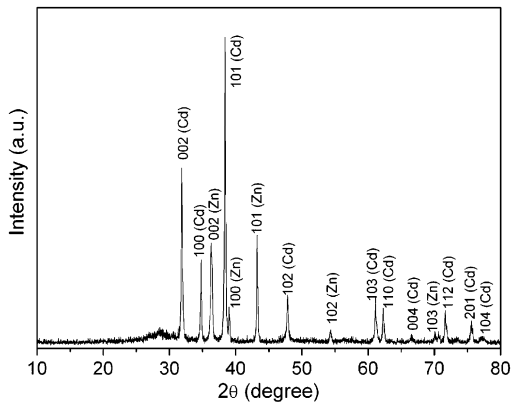

Figure 2. XRD pattern of the synthesized product.

cooled to room temperature, silver-gray products were deposited on the inner wall of the quartz tube.

The collected products were characterized using a scanning electron microscope (SEM, JSM-6700F) and a transmission electron microscope (HRTEM, JEM-3000F) equipped with an energy-dispersive X-ray spectrometer (EDS).

3. Results and Discussion

Thermal evaporation of ZnS and CdS powders resulted in the generation of a dark-gray-colored product on the inner wall of the quartz tube cylinder. The yield of the product is higher than 50% relative to the amount of starting CdS powders used. Figure 2 shows the typical X-ray diffraction (XRD) pattern of the products. It shows two sets of diffraction peaks as hexagonal Zn (JCPDS file: 04-0831) and hexagonal Cd (JCPDS file: 05-0674), respectively.

The general morphology of the as-grown product was examined using scanning electron microscopy (SEM), which reveals that the as-grown products are composed of numerous wirelike nanostructures with typical lengths of several tens of micrometers (Figure 3a). High-magnification SEM image of a single nanowire (Figure 3a, inset) indicates its smooth surface and has diameter of ~70 nm.

Examination by transmission electron microscopy (TEM) and energy-dispersive X-ray spectroscopy (EDS) sheds a light on the microstructural characteristics of the ZnS sheathed Zn−Cd nanowire heterojunctions. Figure 3b shows the TEM image of a typical product obtained in the present route. The clear contrast variations along the structure length suggest that an individual nanowire consists of adjacent nanowires with end-to-end contact of axial segments. The diameters of the nanowires range from 30 to 70 nm. From the images, it also can be seen that all segments in a single nanowire junction are sheathed with a thin layer on their surfaces. The compositions of different segments are checked using EDS taken with an electron nanoprobe (diameter of ~20 nm), and the results show that the dark contrast segment is composed of Cd and the light contrast segment is made of Zn (see the following discussions).

Figure 4a is the TEM image of a typical nanowire junction with a diameter of ~30 nm. EDS spectra were collected from the three spots along the nanowire junction, namely the outer sheathed layer, the dark contrast segment, and the light contrast segment, as indicated with circles in Figure 4a. The corresponding EDS spectra are shown in Figure 4b−d. From these spectra, it can be seen that the outer sheathed layer is composed of Zn and S with a composition of ca. 1:1 (stoichiometry close to ZnS). The dark contrast segment is composed of Cd and the light contrast segment is made of Zn. The C and Cu signals in all

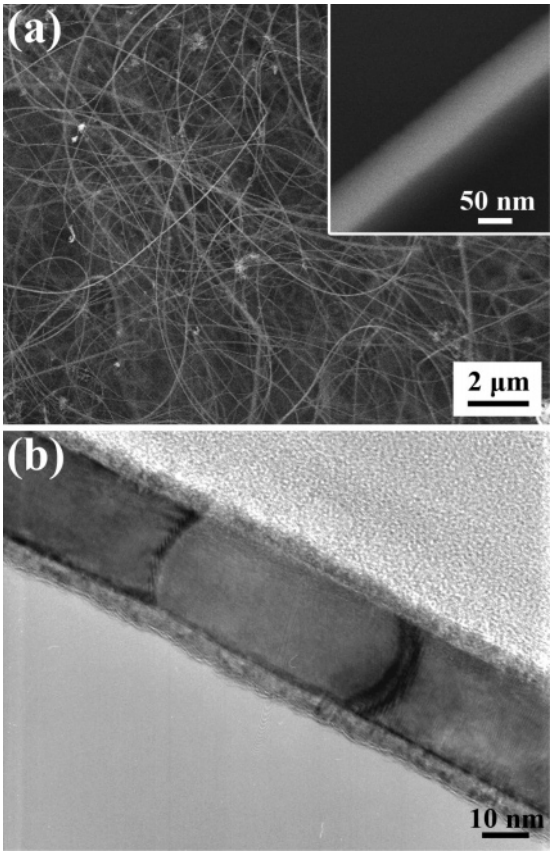

Figure 3. Representative (a) SEM and (b) TEM images of the synthesized ZnS sheathed Zn−Cd nanowire heterojunctions.

three spectra come from the C-coated Cu TEM grid. The EDS results clearly confirm the formation of ZnS sheathed Zn−Cd nanowire heterojunction in the present experimental run.

Figure 5a is the HRTEM image of a single ZnS sheathed Zn−Cd nanowire heterojunction. The obviously varying contrast clearly indicates the several domains within the nanowire. Shown in Figure 5b is the atomically resolved TEM image taken from a Zn subnanowire, which clearly displays its single-crystalline nature. A 0.23 nm separation between the two neighboring lattice fringes corresponds to the $(10\bar{1}0)$ lattice spacing. Figure 5c is the corresponding selected area electron diffraction (SAED) pattern, which shows two sets of diffraction spots. The diffraction pattern can be indexed as that recorded along the [0001] zone axis of hexagonal Zn crystal. The polycrystalline reflections originate from the hexagonal ZnS covering the wire surface. HRTEM image of a Cd subnanowire is shown in Figure 5d. The lattice fringe is separated by 0.25 nm in accord with the (0001) lattice distance of hexagonal Cd crystal. The corresponding SAED pattern in Figure 5e can also be indexed as that recorded along the [0001] zone axis. The HRTEM and SAED results indicate that both the Zn and Cd subnanowires in the heterojunctions are single crystals with the preferred growth direction perpendicular to the $[21\bar{1}0]$ plane. Figure 5f displays the HRTEM image of the outer ZnS crystal sheaths. The discontinuous lattice fringes reveal the polycrystalline nature of the shielding ZnS crystals. The observed lattice spacing is 0.23 nm, corresponding to the $(10\bar{1}2)$ lattice distance of hexagonal ZnS crystal.

Here, a high-resolution transmission electron microscope (HRTEM) image, Figure 6a, is shown to demonstrate the interfacial structure between Cd and Zn metals. It can be seen that Moire contrast background can be found when glancing from Zn to Cd. Figure 6b, the Fourier transform (FT) of Figure

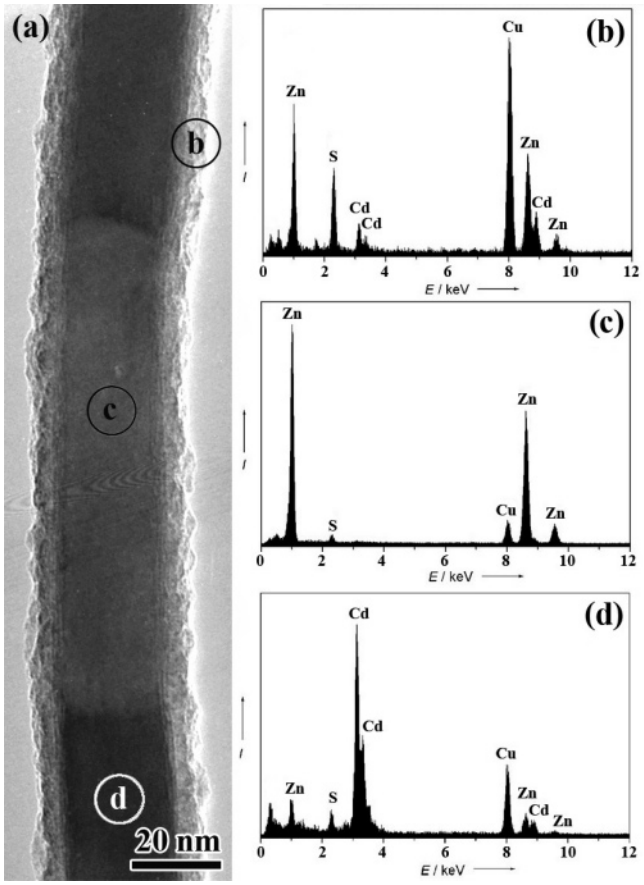

Figure 4. (a) TEM image of a typical ZnS sheathed Zn−Cd nanowire heterojunction. (b−d) Respective EDS spectra taken from the regions indicated in (a).

6a, can be indexed as the diffraction along [0001] zone axis of both Cd (space group $P6_3/mmc$, $a = b = 2.9793$ Å, c=5.6181 Å) and Zn ($P6_3/mmc$, $a = b = 2.665$ Å, $c = 4.947$ Å). The $10\bar{1}0$, $01\bar{1}0$, and $\bar{1}100$ diffractions of Cd and Zn are labeled in Figure 6b (The inner one, 2.58 Å, is of Cd, while the outer one, 2.31 Å, is of Zn). Both the HRTEM image (Figure 6a) and FT diffraction pattern (Figure 6b) show that the Cd and Zn crystals have a crystalline orientation relationship as below,

$$[0001]_{Zn}//[0001]_{Cd} \quad (1a)$$

$$(10\bar{1}0)_{Zn}//(10\bar{1}0)_{Cd} \quad (1b)$$

$$(01\bar{1}0)_{Zn}//(01\bar{1}0)_{Cd} \quad (1c)$$

$$(\bar{1}100)_{Zn}//(\bar{1}100)_{Cd} \quad (1d)$$

Because no angular deviation is found for the above relationship, it is concluded that the relationship is a perfect one and can be explained using the Cd−Zn binary phase diagram[28] and the fabrication procedure of the nanowires. The whole process involves the following reactions: $2ZnS(s) + C(s) \leftrightarrow 2Zn(g) + CS_2(g)$; $2CdS(s) + C(s) \leftrightarrow 2Cd(g) + CS_2(g)$; $ZnS(s) \leftrightarrow ZnS(g)$. At high reaction temperature, solid ZnS and CdS were first reduced to Zn (bp = 907 °C)[18] and Cd vapors by carbon (coming from the graphite crucible). The newly generated Zn and Cd vapors were transported by the carrying gases (Ar in this case) to the low-temperature region where they deposited on the inner wall of the quartz tube in the form of liquid droplets. The Cd−Zn binary phase diagram shows that Cd and Zn metal can dissolve with each other in any ratio as a mixed liquid at a temperature higher than 419.58 °C.[28] In the experiment, at the

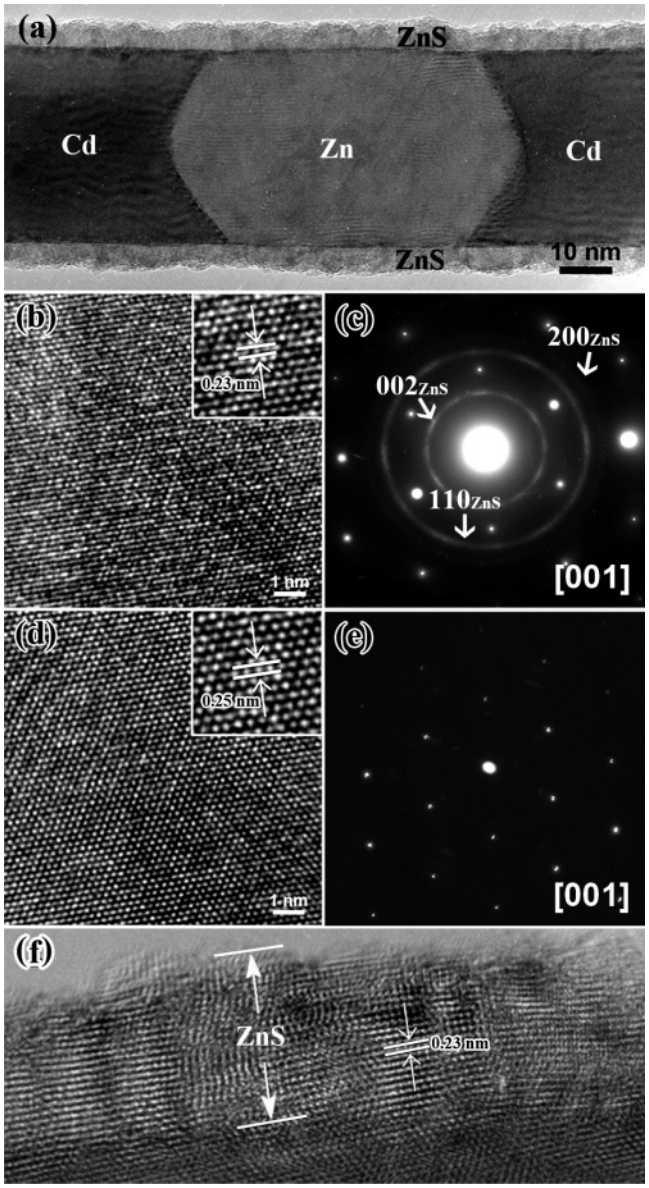

Figure 5. (a) TEM image of the typical part of a nanowire heterojunction, (b) HRTEM image, and (c) SAED pattern of a Zn subnanowire in the heterojunction. (d) HRTEM image and (f) SAED pattern of a Cd subnanowire in the heterojunction. (f) HRTEM image showing the sheathed ZnS on the heterojunction surface.

end of the reaction, the temperature gradually decreased when we shut down the electronic power. Once the temperature decreased to 419.58 °C, Zn metal (containing Cd with an amount less than 1.46% atom-ratio) and Zn−Cd solid solution separated out from the mixed metal liquid. In the meantime, the Zn metal crystallized spontaneously. When temperature decreased to 321.108 °C, Cd metal (containing Zn with an amount less than 4.35% atom-ratio) began to separate out from the mixed metal liquid and started to crystallize. It is reasonable that the growth of Cd crystal (containing Zn) cannot be independent of the preexisting Zn crystal (containing Cd) and its orientation is controlled by the preexisting Zn crystal. In fact, the growth of Cd is a heteroepitaxial one in Zn metal. When the orientation adopts the relationships (eq 1a−d), the misfit is the smallest (10.55% along any direction vertical to the c direction and 11.94% along the c direction) compared with other orientation relationships. Figure 6c is the inverse Fourier transform (IFT) of the diffractions around the center transmission spot in Figure 6b. It shows the Moire fringes with a periodic change of white

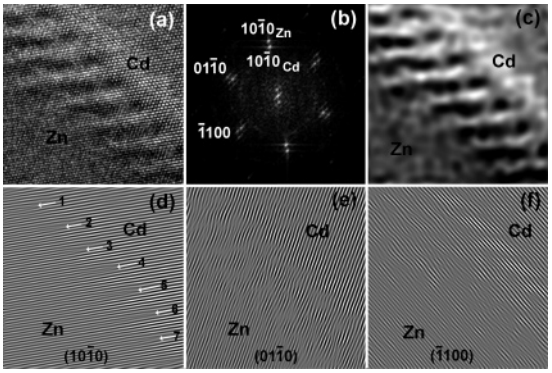

Figure 6. (a) HRTEM image around the Zn−Cd interfacial region. (b) FT of the HRTEM image. (c) IFT of the diffraction around the center transmission spot. (d) IFT of $(10\bar{1}0)$Zn and $(10\bar{1}0)$Cd diffraction in Figure 5b. Periodic misfit dislocations "1", "2", "3", "4", "5", "6" and "7" are labeled by the arrowheads. (e) IFT of $(01\bar{1}0)$Zn and $(01\bar{1}0)$-Cd diffractions in Figure 5b. (f) IFT of $(\bar{1}100)$Zn and $(\bar{1}100)$Cd diffractions in Figure 5b.

and dark contrast clearly, the same as that in Figure 6a. A careful counting in Figure 6a reveals that the Moire fringes have an average period $m \sim 9.4$ times of the $(10\bar{1}0)_{Zn}$ d spacing. It is very close to the ideal period $m \sim 9.49$, which is determined by the equation $D = md_2 = d_1d_2/(d_1 - d_2)$ (where d_1 and d_2 are the d spacings of $(10\bar{1}0)_{Cd}$ and $(10\bar{1}0)_{Zn}$, respectively).[29] Figure 6d is the IFT of $(10\bar{1}0)_{Zn}$ and $(10\bar{1}0)_{Cd}$ diffraction in Figure 6b, where "1", "2", "3", "4", "5", "6", and "7" periodic misfit dislocations are labeled by the arrowheads. The distance between two neighboring misfit dislocations is $n \sim 9$ times of d spacing of $(10\bar{1}0)_{Zn}$ plane, except $n \sim 8$ between the "3" and "4" misfit dislocations. By glancing along the $(10\bar{1}0)$ plane in Figure 6a, it can be found that the center of Moire dark fringes in Figure 6a and c correspond to the misfit dislocations in Figure 6a and d at "4", "5", "6", and "7" misfits dislocations. At "1", "2", and "3" misfit dislocations, the center of Moire dark fringes are outside of the misfit dislocations by 3, 2, and 1 times the $(10\bar{1}0)_{Zn}$ d spacing, respectively. Between $(01\bar{1}0)_{Zn}$ and $(01\bar{1}0)_{Cd}$ planes, there are also some misfit dislocations, see in Figure 6e, the IFT of $(01\bar{1}0)_{Zn}$ and $(01\bar{1}0)_{Cd}$ diffractions in Figure 6b. However, the dislocations exist in a nonperiodic disordered state. We believe that the periodic misfit dislocations in Figure 6d release a majority of strain between Zn and Cd and the disordered misfit dislocations in Figure 6e release the remaining strain on the base plane vertical to [0001] axis. Parallel to the $(01\bar{1}0)$ planes in Figure 6a and e, there are not obvious periodic Moire contrast, which may be offset by the disordered misfit dislocations on the $(01\bar{1}0)$ plane. Figure 6f is the IFT of $(\bar{1}100)_{Zn}$ and $(\bar{1}100)_{Cd}$ diffractions. The d spacings of the $(\bar{1}100)$ plane in the interfacial region might have some change because its corresponding diffraction in Figure 6b is not a spot but an elongated line vertical to $(\bar{1}100)$ plane. This phenomenon should be originated from the Kanzaki force acting on the interfacial atoms, which is different from the atoms in Zn and Cd inner regions.[30] All of parts d−f of Figure 6 show that the interfacial region between Zn and Cd have a structure with an order worse than the Zn and Cd inner regions.

The schematics in Figure 7a−d are shown here to explain the coincidence between Zn and Cd crystals. Figure 7a is a unit cell of Zn (or Cd). Hexagonal Zn or Cd belongs to the space group: $P6_3/mmc$. In a unit cell of Zn (or Cd), it contains 2 atoms, one in the (0,0,0) site and another in the ($^1/_3$, $^2/_3$, $^1/_2$) site, where $a = b$ and the angle between a and b is 120°. The angle between a and c, b and c are 90°. In the Zn/Cd system, because the eutectic temperature is 266 °C, their interface should be sharp

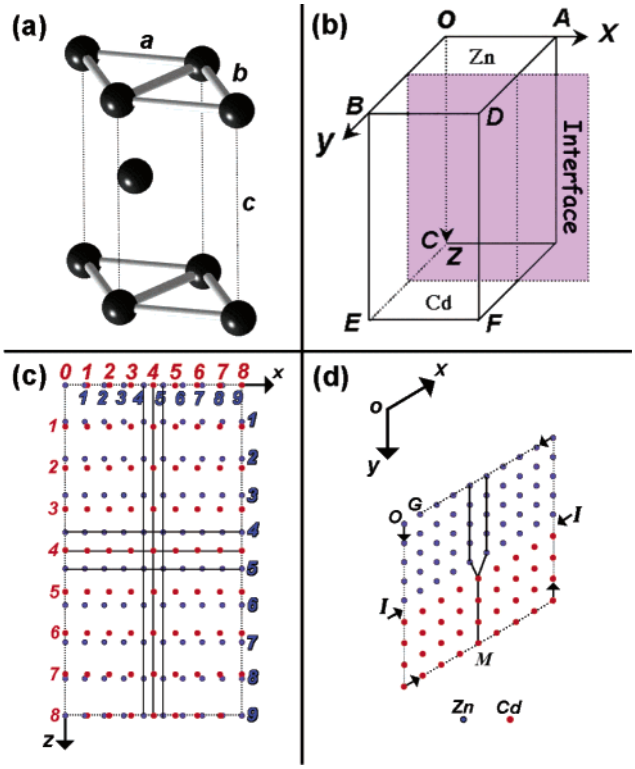

Figure 7. (a) Schematic of a unit cell of Zn (or Cd). (b) Schematic of a sharp Zn/Cd interface on the $(\bar{1}100)$ plane. (c) Plan view of the interface. Zn and Cd atoms are in two different depths along oy direction. (d) Cross-sectional view of the interface along [0001] direction. "I" and "M" indicate the interface and misfit dislocation between Zn and Cd, respectively.

in element at room temperature. However, the interface of the synthesized heterojunctions here is not flat but embossing or overlapping in a large contact area, which is proven by the Moire fringes in Figure 6a and the dislocations "1", "2", "3", "4", "5", "6", and "7" on an arc in Figure 6d. To study the Zn/Cd interface, we assumed that the interface is both sharp in element and flat in shape on a small contact area, as illustrated in schematic Figure 7b. When we observed the Zn/Cd contact interface plane (plan view), the coincidence between Zn and Cd can be drawn as in Figure 7c (Zn and Cd atom are in two different depths viewing along oy direction). Along ox and oz directions, the misfits are 0.632% and 0.9432% when 9 Zn atoms fit 8 Cd atoms, respectively. Because the "0", "1", "2", "3", "6", "7", "8", and "9" Zn atoms try to face "0", "1", "2", "3", "5", "6", "7", and "8" Cd atoms straightly, respectively, the $(10\bar{1}0)_{Zn}$ (//OBEC plane in Figure 6b) and $(0001)_{Zn}$ (//OBDA plane) planes and $(10\bar{1}0)_{Cd}$ and $(0001)_{Cd}$ planes containing these atoms will extend and shrink, respectively. This point can be confirmed by glancing the interfacial fringes in Figure 6d for the $(10\bar{1}0)_{Zn}$ and $(10\bar{1}0)_{Cd}$ planes. However, the $(10\bar{1}0)_{Zn}$ and $(0001)_{Zn}$ planes and $(10\bar{1}0)_{Cd}$ and $(0001)_{Cd}$ planes containing "4" and "5" Zn atoms and "4" Cd atoms (marked by 6 solid lines in Figure 7c) cannot face straightly to each other, and a misfit dislocation occurs. We can describe the misfit dislocation as following: a Burgers circuit is drawn along OBDAO in Figure 7b and a Burgers partial vector $\vec{a}$ (one side in the hexagon of (0001) plane) was obtained, seeing OG in Figure 7d. It is very similar to the diamond film on silicon substrate, where the Burgers vector $a/2[01\bar{1}]$ for the misfit dislocation is also one side in the hexagon of the (111) plane.[31] Another Burgers circuit can be drawn along OCEBO, and this partial vector $\vec{c}$ was also obtained. Then the misfit dislocation has a Burgers

vector as $\vec{a} + \vec{c}$ in a cell with $8a_{Cd} \times L \times 8c_{Cd}$ (or $9a_{zn} \times L \times 9c_{Zn}$) volume ($L$ is arbitrary). If we describe the interface using a near-coincidence site lattice (NCSL) concept,[31] we can find that 49 Zn atoms fit 49 Cd atoms in the $8a_{Cd} \times 8c_{Cd}$ (or $9a_{Zn} \times 9c_{Zn}$) area, then the parameter for the NCSL should be $\sum_{Zn}$ 81/49:$\sum_{Cd}$ 64/49, i.e., $\sum_{Zn}$ 1.653:$\sum_{Cd}$ 1.306.

4. Conclusion

In summary, we have successfully synthesized ZnS sheathed Zn−Cd nanowire heterojunctions by a simple one-step thermochemical process. Both the Zn and Cd subnanowires are single crystals with the preferred growth directions perpendicular to the $[2\bar{1}\bar{1}0]$ plane, whereas the sheathed ZnS is polycrystalline with a thickness of ca. 5 nm. Zn/Cd interface structure was thoroughly studied by high-resolution transmission electron microscopy, which shows that the Cd and Zn have a crystalline orientation relationship as $[\bar{0}\bar{0}01]_{Zn}//[\bar{0}\bar{0}01]_{Cd}$, $(10\bar{1}\bar{0})_{Zn}//(10\bar{1}\bar{0})_{Cd}$, $(01\bar{1}\bar{0})_{Zn}//(01\bar{1}\bar{0})_{Cd}$, and $(\bar{1}100)_{Zn}//(\bar{1}100)_{Cd}$. Within a single nanowire heterojunction, there exist several kinds of heterojunctions including metal−semiconductor (Zn−ZnS, Cd−ZnS) subheterojunctions and metal−metal (Zn−Cd) subheterojunctions, which may possess some unique properties and find potential applications in the fabrication of nanodevices.

Acknowledgment. We thank Dr. D. Chen at the Photocatalytic Center, NIMS, Japan for sample characterizations. We also thank Dr. J. Q. Hu, and J. H. Zhan for helpful discussions.

References and Notes

(1) Iijima, S. *Nature* **1991**, *354*, 56.
(2) Rao, C. N. R.; Deepak, F. L.; Gundiah, G.; Govindaraj, A. *Prog. Solid State Chem.* **2003**, *32*, 5.
(3) Xia, Y. N.; Yang, P. D.; Sun, Y.; Wu, Y.; Mayers, B.; Gates, B.; Yin, Y.; Kim, F.; Yan, H. Q. *Adv. Mater.* **2003**, *15*, 353.
(4) Sun, Y.; Fuge, G. M.; Fox, N. A.; Riley, D. J.; Ashfold, M. N. R. *Adv. Mater.* **2005**, *17*, 2477.
(5) Pan, Z. W.; Dai, Z. R.; Wang, Z. L. *Science* **2001**, *291*, 1947.
(6) Chen, D.; Tang, K. B.; Liang, Z. H.; Liu, Y. K.; Zheng, H. G. *Nanotechnology* **2005**, *16*, 2619.
(7) Sze, S. M. *Physics of Semiconductor Devices*; Wiley-Interscience: New York, 1981.
(8) Lauhon, L. J.; Gudiksen, M. S.; Lieber, C. M. *Philos. Trans. R. Soc. London, Ser. A* **2004**, *362*, 1247.
(9) Lauhon, L. J.; Gudiksen, M. S.; Wang, D. L.; Smith, D. C.; Lieber, C. M. *Nature* **2002**, *420*, 57.
(10) Kuang, Q.; Jiang, Z. Y.; Xie, Z. X.; Lin, S. C.; Lin, Z. W.; Xie, S. Y.; Huang, R. P.; Zheng, L. S. *J. Am. Chem. Soc.* **2005**, *127*, 11777.
(11) Gudiksen, M. S.; Lauhon, L. J.; Wang, J.; Smith, D. C.; Lieber, C. M. *Nature* **2002**, *415*, 617.
(12) Wu, Y. Y.; Fan, R.; Yang, P. D. *Nano Lett.* **2002**, *2*, 83.
(13) Bjork, M. T.; Ohlsson, B. J.; Sass, T.; Persson, A. I.; Thelander, C.; Magnusson, M. H.; Deppert, K.; Wallenberg, L. R.; Samuelson, L. *Nano Lett.* **2002**, *2*, 87.
(14) Manna, L.; Scher, E. C.; Li, L. S.; Alivisatos, A. P. *J. Am. Chem. Soc.* **2002**, *124*, 7136.
(15) Li, Q.; Wang, C. R. *J. Am. Chem. Soc.* **2003**, *125*, 9892.
(16) He, R. R.; Law, M.; Fan, R.; Kim, F.; Yang, P. D. *Nano Lett.* **2002**, *2*, 1109.
(17) Zhan, J. H.; Bando, Y.; Hu, J. Q.; Liu, Z. W.; Yin, L. W.; Golberg, D. *Angew. Chem., Int. Ed.* **2005**, *44*, 2140.
(18) Hu, J. Q.; Bando, Y.; Zhan, J. H.; Golberg, D. *Adv. Mater.* **2005**, *17*, 1964.
(19) Hu, J. Q.; Li, Q.; Meng, X. M.; Lee, C. S.; Lee, S. T. *Chem. Mater.* **2003**, *15*, 305.
(20) Obare, S. O.; Jana, N. R.; Murphy, C. J. *Nano Lett.* **2001**, *1*, 601.
(21) Mayya, K. S.; Gittins, D. I.; Dibaj, A. M.; Caruso, F. *Nano Lett.* **2001**, *1*, 727.
(22) Shen, G. Z.; Bando, Y.; Tang, C. C.; Golberg, D. *J. Phys. Chem. B* **2006**, *110*, 7199.
(23) Liu, C.; Li, R. W.; Belik, A.; Golberg, D.; Bando, Y.; Cheng, H. M. *Appl. Phys. Lett.* **2006**, *88*, 043105.
(24) Hu, J. Q.; Bando, Y.; Zhan, J. H.; Yuan, X. L.; Sekiguchi, T.; Golberg, D. *Adv. Mater.* **2006**, *17*, 971.
(25) Wang, J. G.; Tian, M. L.; Kumar, N.; Mallouk, T. E. *Nano Lett.* **2005**, *5*, 1247.
(26) Hu, P.; Liu, Y. Q.; Fu, L.; Cao, L. C.; Zhu, D. B. *Chem. Commun.* **2004**, 556.
(27) *CRC Handbook of Chemistry and Physics*, 3rd electronic edition; CRC: Cleveland, OH, 2000.
(28) Massalski, T. B.; Okamoto, H.; Subramanian, P. R.; Kacprzak, L.; Scott, W. W.; Fleming, M. A.; Boring, R.; Losasso, A. *Binary Alloy Phase Diagrams*, 2nd ed.; ASM International: Materials Park, OH, 1990.
(29) Hirsch, P. B.; Howie, A.; Nicholson, R. B.; Pashley, D. W. *Electron Microscopy of Thin Crystals*; London: Butterworths, 1965; p 169.
(30) Kanzaki, H. *J. Phys. Chem. Solids* **1957**, *2*, 24.
(31) Jia, C. L.; Urban, K.; Jiang. X. *Phys. Rev. B* **1995**, *52*, 5164.